AD 273 817

62-2-6

AE 62-0218 M
Space Science Laboratory

Methods of Analysis of Microwave Scattering from Wakes of Hypervelocity Projectiles

W. R. Bradford
B. H. Siperly

12 February 1962

1760

GENERAL DYNAMICS | ASTRONAUTICS

RDM62-010

#310

AE 62-0218M
Space Science Laboratory

Methods of Analysis of Microwave Scattering from Wakes of Hypervelocity Projectiles

W. R. Bradford
B. H. Siperly

12 February 1962

This work was supported by the Advanced Research Projects Agency through the Army Rocket and Guided Missile Agency under Contract Nos. DA-04-495-ORD-3112 and -3383 as part of Project Defender.

RDM62-010

CONTENTS

ILLUSTRATIONS

ABSTRACT

Interpretation of ballistic range experimental results is outlined for tests conducted with 20mm blunt polyethylene projectiles. A detailed theoretical treatment of forward-scattered microwave signals from a dilute plasma column is given. Estimates of ionized wake diameters are made from schlieren photographs of the flow field and are related to back-scattered microwave signals. Returns from perfect scattering rods are compared to returns from an ionized wake in the overdense case. Decay rate changes are noted on microwave returns from an ionized wake and may indicate the transition from laminar to turbulent flow. An indication of "roughness" and separation of scattering centers is shown. General plans for future tests are given.

I. INTRODUCTION

Controlled experiments conducted in ballistic ranges greatly aid the investigations of the phenomena of high velocity flight. Most flight parameters can be simulated by careful control of scaled models and test conditions. In addition, many experiments can be conducted with savings in time and cost. Full utilization of ballistic ranges has not been prevalent, primarily due to the difficulty of interpreting the results of tests.

The phenomena of re-entry of a high velocity body are complex, and many factors influence the results observed. However, gross effects due to changing pressure, velocity of the body, body geometry, and body composition can be readily observed. One of the best techniques for studying these effects is by use of microwave diagnostics.

General Dynamics has studied re-entry phenomena by means of ballistic range experiments over the last several years. The purpose of this report is to update the analysis and interpretation of the results of tests made at the NASA Ames Ballistic Range. This analysis is then applied to the measurements, and results are presented. Recommendations for further analysis are made from the information known.

II. THEORETICAL ANALYSIS

Consider an ionized column behind a hypervelocity body illuminated by a point source of microwave energy and examined at an equally distant point, coplanar with the source point and the column axis. Polarization is horizontal. Forward-scattering measurements use the power received due to superposition of applied and scattered fields. These results permit a computation of the number of electrons in the column per unit distance along the column's axis. Back-scattering measurements are instrumented so the applied field is cancelled out. The measured reflection coefficient gives the radial distribution of electrons as the solution of an integral eqation.

The parameter obtained directly from the forward-scattering measurements is the ratio P_f/P_{fo} of microwave power received through the ionized column to that outside the column. Let X_o be the common distance of phase centers of the two microwave horns from the column's axis and λ be the free-space wavelength of the microwave energy employed. Appendix A gives the detailed analysis, resulting in the expression

$$q = C \left[1 - \sqrt{2\left(\frac{P_f}{P_{fo}} - \frac{1}{2}\right)} \right] \qquad (1)$$

where

$$C = 1.8 \sqrt{\frac{X_o}{\lambda}} \times 10^{12} \text{ electrons/cm.}$$

Here q is the linear charge density of electrons in the ionized column. This includes all electrons in the column between two planes normal to the column's axis and separated by unit distance. The equation for q is in terms of the measured power ratio and the geometry of the

particular system. C and P_f/P_{fo} can be accurately measured. Figure 1 shows a plot of Equation (1). Notice that the plot does not include the possibility of a focussing effect, $P_f > P_{fo}$. This has never been observed in the experiments for the dilute column assumed in the analysis. The fact that q is bounded, $q \leq C$, is probably a reflection of the dilute column assumption.

Back-scattering measurements use the same horn for transmission and reception. The parameter measured is the reflection coefficient defined by Eshleman[1] as

$$\rho_B = \sqrt{\frac{\pi kx_o}{2}} \cdot \frac{\text{scattered electric field magnitude at antenna}}{\text{applied electric field magnitude at column's axis}}$$

The analysis of Appendix A relates this to the (volume) density, $N(\xi, Z)$, of electrons in the column. The relation obtained is

$$\rho_B = A \int_0^a N(\xi, 0)\, J_o(2k\xi)\, \xi\, d\xi \qquad (2)$$

Here $A = 3.93 \times 10^{-12}$ cm/electron, $k = \omega/c$ is the free space wavelength constant and ξ is the off-axis distance, within the column of radius a, to a local point where the electron density is $N(\xi, 0)$. Appendix A shows this geometry.

Barthel[2], using a plane wave source, obtains the same result as Equation (2), except his A is $\sqrt{2}$ times that obtained here for the point source. Since $N(\xi, 0)$ vanishes for $\xi > a$, by definition, he is able to extend the upper integration limit to infinity. He then applies the Fourier-Bessel transform to obtain

$$N(\xi, 0) = \frac{4}{A} \int_0^\infty \rho_B(k)\, J_o(2k\xi)\, k\, dk. \qquad (3)$$

The formal solution of Equation (3) requires an experimental knowledge of ρ_B at all microwave frequencies. The manner in which this integral may be approximated, using a small number of experimental frequencies to give corresponding values of ρ_B, is discussed in Reference 2.

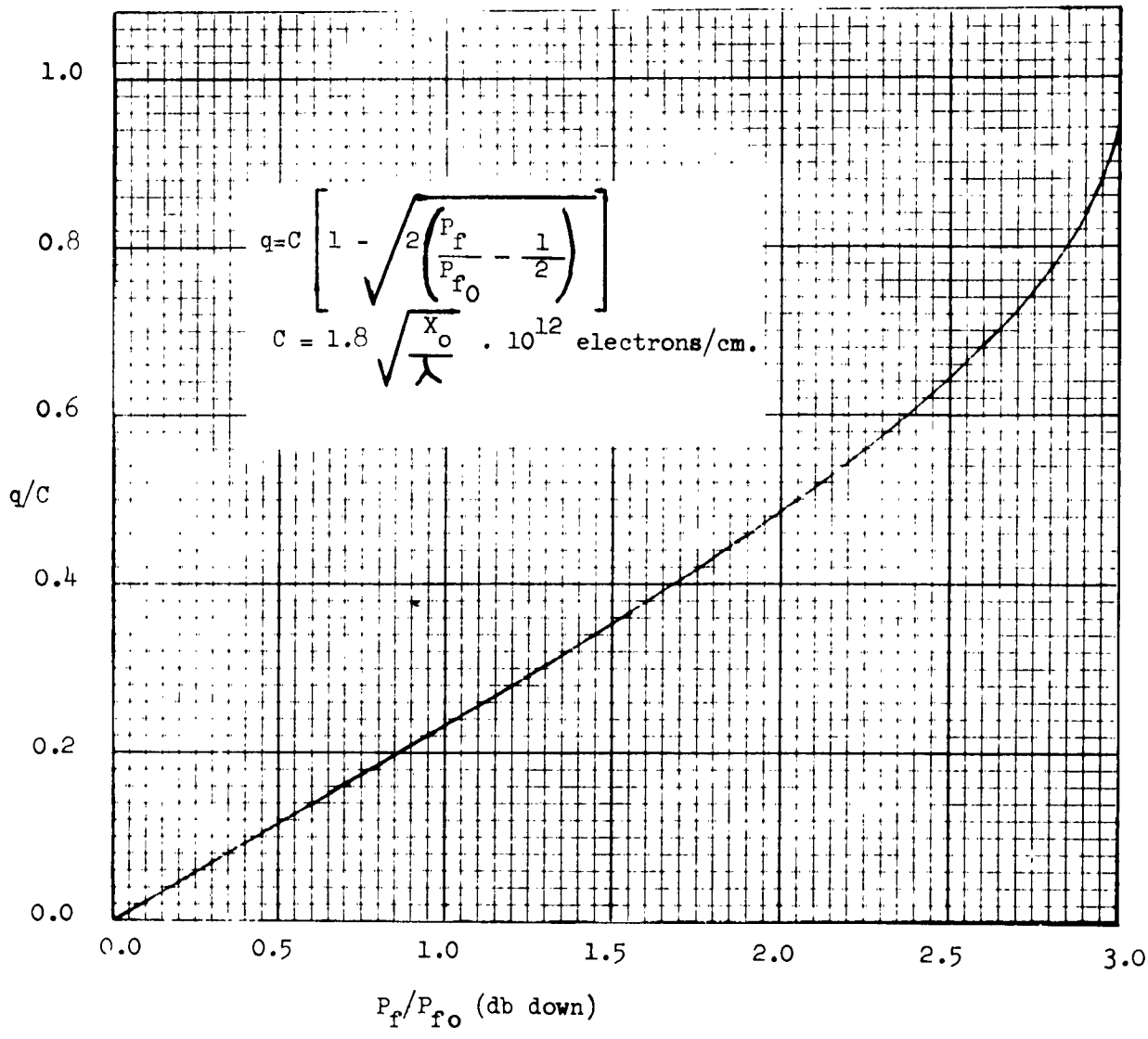

Figure 1. Linear Charge Density as a Function of Attenuation of Transmitted Power

As explained in Reference 2, the electron scattering theory should be verified by the forward-scattered results before we attempt to evaluate $N(\xi, 0)$ by approximating Equation (3). This verification involves getting consistent results from Equation (1) for various microwave frequencies. This, in turn, demands that we have a clear understanding of the assumptions used in Appendix A.

The dilute column assumption is introduced as inequality (A-1) in Appendix A. This assumption is treated in detail in Appendix B, which considers phase as well as attenuation. We find (inequalities B-12) the plasma frequency, f_p, the microwave frequency, f, and the ambient pressure, p(mm Hg), must comply with the relations

$$\left(\frac{f_p}{f}\right)^2 << 1 + 0.91\left(\frac{p}{fx10^{-9}}\right)^2 \qquad (4)$$

$$p \leq 2.1\ (fx10^{-9}).$$

Thus, the pressure at which the tests are conducted must be about 10 mm Hg or less for the results to be applicable to analysis.

The second assumption is introduced as inequality (A-2) in Appendix A. This states that the diameter of the column subtends a negligible angle at either horn for all purposes except phase.

The third assumption, inequality A-3, states that the column diameter must be very small compared to the geometric mean of the horn-to-column's axis distance and the free-space half-wavelength. This means the column-to-horn distance, if initially marginal, must increase in proportion to the frequency of the microwave used.

The fourth assumption, used in the stationary phase integrations of Equations A-8 and A-18, is that a horn's principal E-plane power pattern and the radial distribution of electrons should vary slowly with change in position along the column axis, compared to phase oscillations associated with a line from the source to the electron.

Besides the four assumptions detailed above, we shall eventually be concerned with further assumptions associated with approximate solutions of Equation (3) above. Possible approaches are suggested by Reference 2. It is expected that several approximation techniques may be checked out as back-scattering data become available at several microwave frequencies.

III. EXPERIMENTAL RESULTS

From the theoretical treatment, as detailed in Appendixes A and B, it seemed appropriate to analyze the forward-scattered returns and get correlation for a number of shots as the first step, so that confidence would be felt in the approach as applied to the range geometry.

Figure 2 shows the linear charge density of a large number of tests. The models were polyethylene cylinders 0.8 in. in diameter by 0.4 in. long with a 0.6 in. radius face. All were fired at a range pressure of 1 mm Hg. The linear charge density is plotted as a function of the distance behind the body. The values of linear charge density were obtained from Equation (1). The decay is a power law of distance behind the body, being a different power at each velocity.

The magnitude of slopes in Figure 2 fit equally a fourth or fifth power dependence on model speed. A wider range of model speeds is required for a reliable empirical fit.

By using the analysis to present the data in the form of Figure 1, one can possibly obtain some relationship to describe the wake and phenomena in a simple enough form to be useful; and a macroscopic model may be evolved. An empirical description of the linear charge density was derived from the data in Figure 2. By use of such data, one could possibly predict the charge density within the range of interest.

A series of such tests could be made under various test conditions to obtain the gross effect of varying parameters. After a series of such tests, a descriptive model could be determined.

The data plotted in Figure 2 was obtained at only one frequency. To adequately cover a wide range of electron densities on a given test, many frequencies would be required. Each frequency would have the

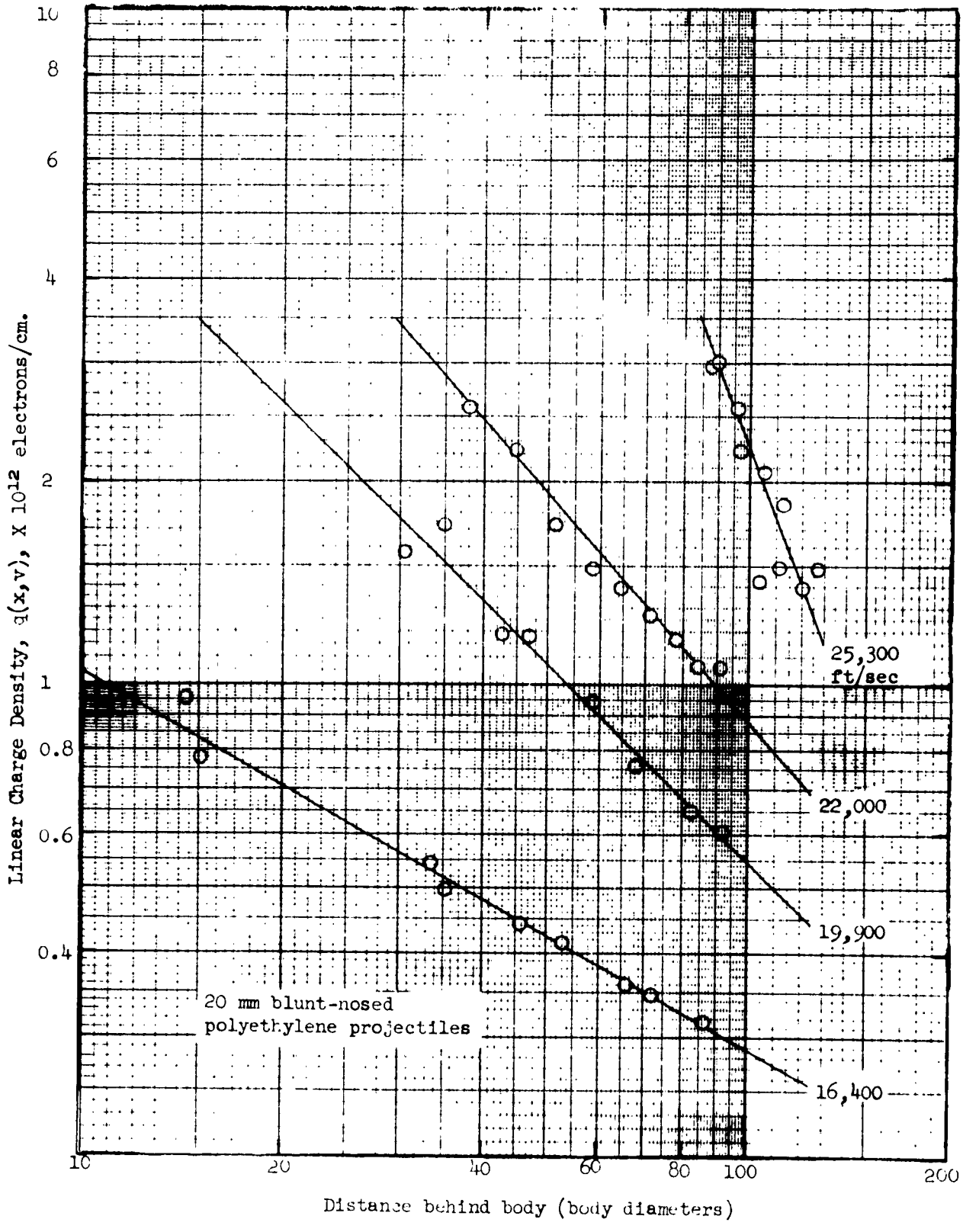

FIGURE 2. LINEAR CHARGE DENSITY. Computed from power transmitted through wake at 5 Gcs and 1 mm Hg ambient pressure using Eq. (1). This approximation involved in Eq. (1) have been estimated to give rise to less than a 25% error in the value of q if [illegible].

dilute column model met at some distance behind the body if the frequency were below the plasma frequency at some point in the wake. The frequencies would be chosen so that the model described in Appendix A would be applicable for a given frequency at all times of the test and that each frequency range would overlap the next frequency range. A continuous record of linear charge density could then be obtained.

In addition to the method of analysis given in the appendix, other means are available to obtain information. Comparison to perfect scattering rods can be made if the ionized wake is "overdense" or completely scattering to a given frequency. Thus, the dilute column model may be valid at a given frequency, while at the same time the rod comparison is valid at another frequency.

The measured returns of a series of rods are shown in Figure 3. The range of values obtained results from the method of inserting the rods on-axis in the range section. If a comparison is made of these returns to those obtained from a wake, one may determine if the wake were overdense. This would require that an estimate of the wake diameter be made from the knowledge of the flow field behind the body. As the returns from the ionized wake drop below the return from a rod whose diameter is estimated from the flow field, one can conclude that the estimate is too great or that the trail has become "underdense". At this point in the trail we cannot tell then if it is "overdense" or "underdense". However, the dilute column model developed in Appendix A fixes the lower limit of overdense uncertainty. There exists then, an area bounded by the known underdense and overdense trails, as determined by perfect-scattering rod measurements.

Back-scattered returns for three shots at 1 mm Hg covering a range of velocities are shown in Figure 4. The exponential decay is easily seen as well as the decay rate change. Values of rod returns are indicated for a range of rod diameters.

As indicated previously, an analysis such as this must be done with data from several microwave frequencies and consistency shown between the frequencies. Consistency would tend to verify the dilute column model developed in Appendix A. The choice of frequencies to employ must, of course, be determined by the range of test conditions used on ballistic

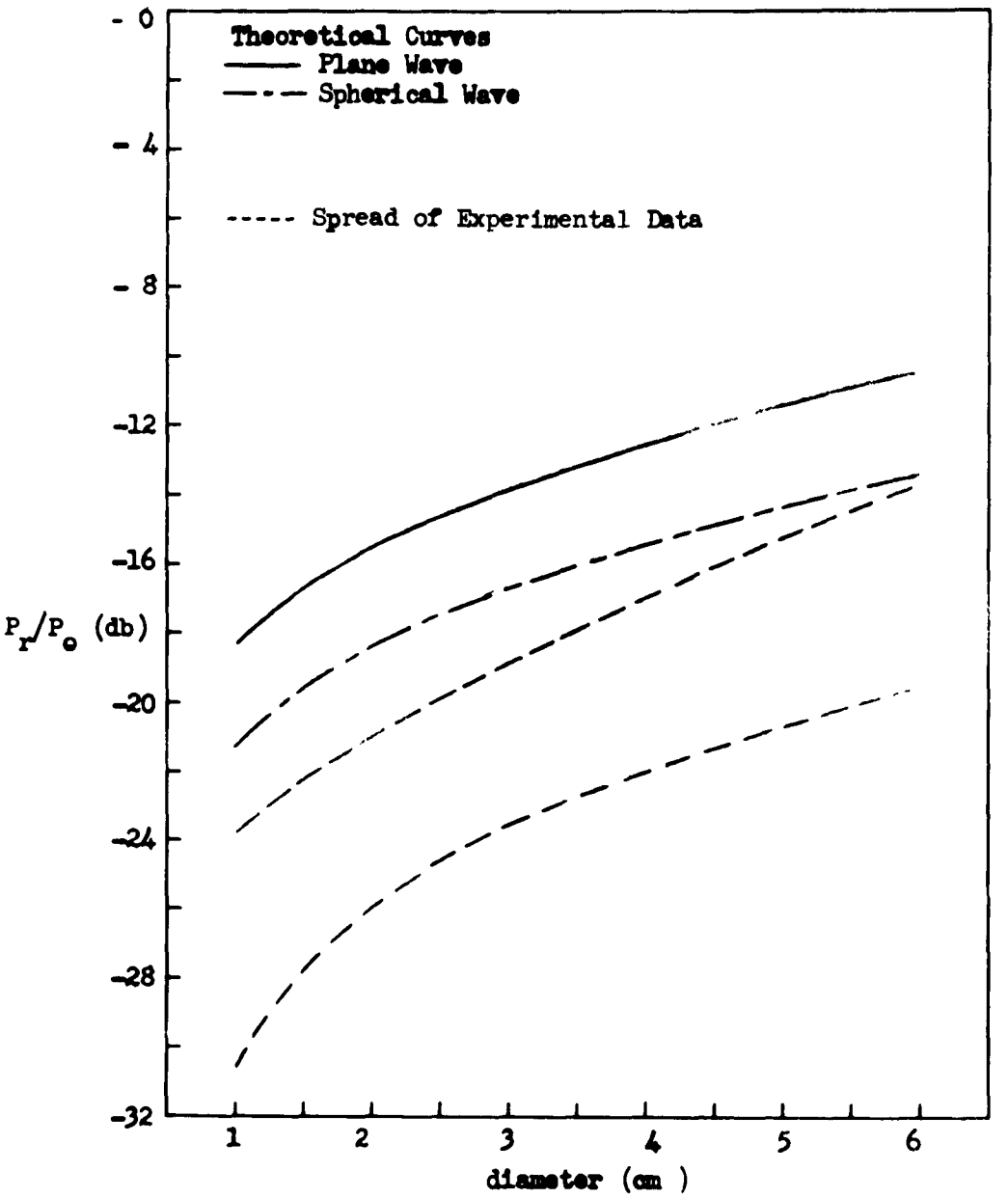

Figure 3. Reflected Returns from Rods, 5 Gcs

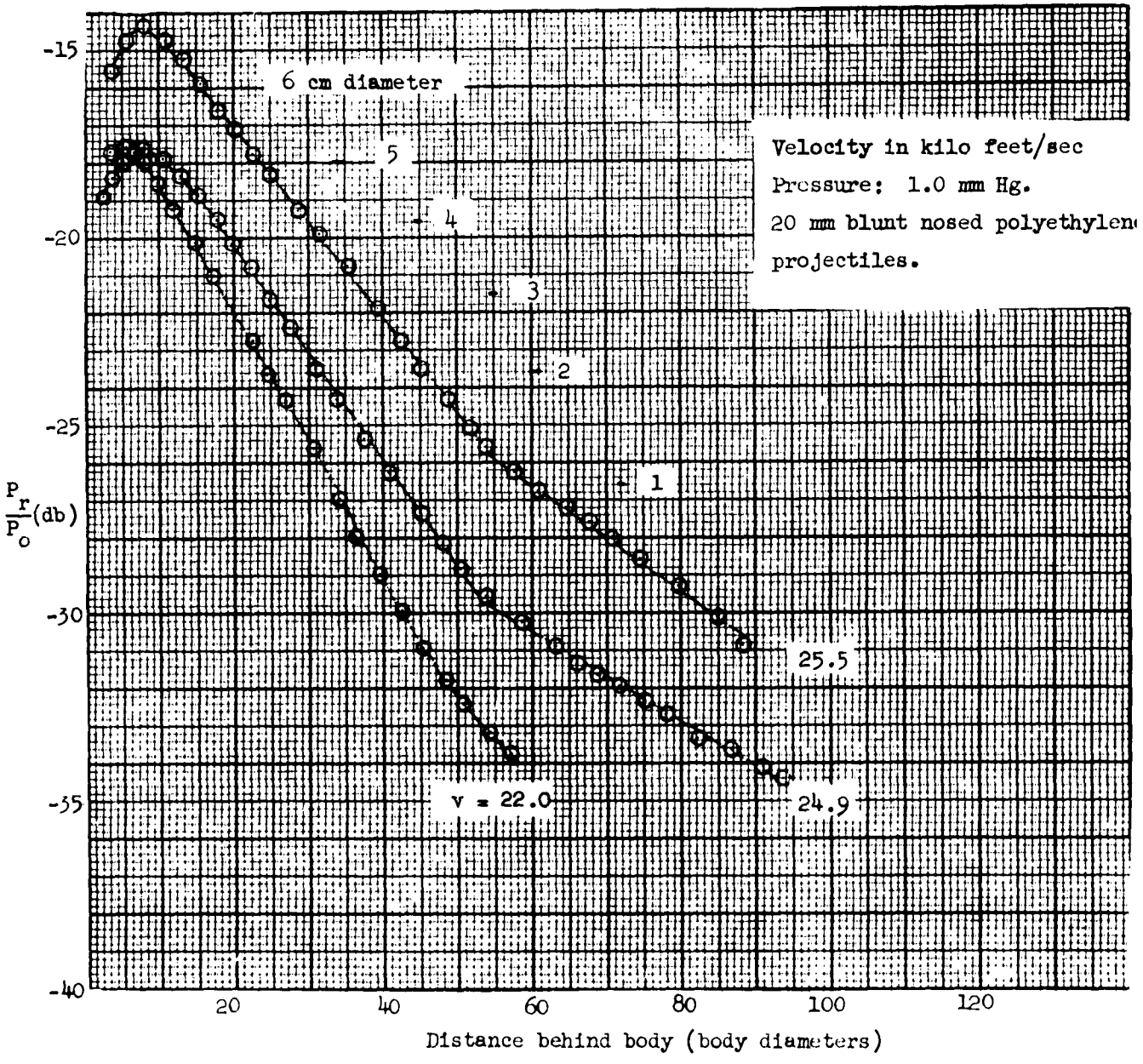

Figure 4. Reflections Coefficients of Wakes, 5 Gcs

ranges to adequately cover the range of electron densities produced.

The estimate of wake diameter maxima as determined by the flow field can be obtained from schlieren photos. A high-speed continuous schlieren record is made of all firings. Any irregularities that may occur in the flow field due to model orientation, model damage, or other individual shot peculiarity, are easily determined. Records are obtained by schlieren techniques to pressures as low as 7 mm Hg as regards the viscous wake and well below 1 mm Hg for the bow and recompression shocks.

Exponential decay of the reflected microwave return is observed on many of the firings, particularly those known to be overdense. Many decay at a particular exponential rate for an appreciable distance behind the body, then abruptly, the decay rate changes, though remaining exponential for another long distance behind the body. Effects similar to these are observed by Hidalgo[3] from luminosity measurements. Coupled with drum camera data, Hidalgo has interpreted these decay rate changes as the point behind the body where transition from laminar to turbulent wake flow occurs. Such an explanation may be applicable to the radar returns. For the model body diameter employed at the NASA ballistic range, the pressure at which laminar-to-turbulent flow occurs is probably in the range of 5 to 10 mm Hg. At this pressure the turbulent wake is clearly visible on a schlieren photo and protusions may possibly be noted at the point where transition occurs. No change in decay rates of the returns are observed on firings above 10 mm Hg ambient range pressure. More data on firings at 5 to 10 mm Hg are needed before one can conclude that transition is observed on radar returns.

Figure 5 shows the results of a test conducted at a pressure of 1 mm Hg and a velocity of 25,700 ft/sec. The comparison can be made between the 5-Gcs returns and luminosity measurements in the 3300-4000Å region. The point behind the body where the decay rate changes abruptly is about the same point. Correlation of returns strongly suggests that optical signatures may be related to radar signatures.

Amplitude fluctuations of the forward- and back-scattered microwave signals are noted on all firings, but the point behind the projectile where they occur varies, being dependent on pressure and velocity. This

Blunt Polyethylene Model

Pressure = 1.0 mm Hg Velocity = 25,700 ft/sec

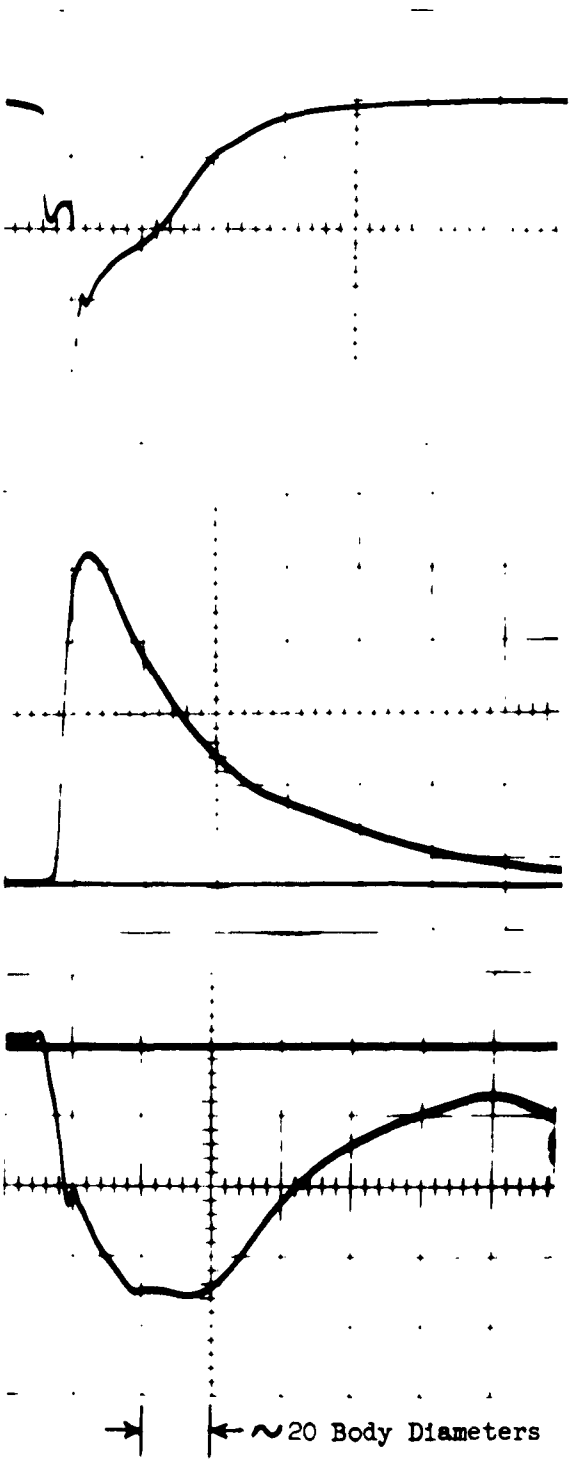

Figure 5. Comparison between microwave Signals and Radiation Intensity

is true of all microwave frequencies used. On tests where luminosity measurements are obtained and the flow is determined to be laminar well behind the body, the return is a smooth curve. No fluctuations are noted then for hundreds of body diameters and then, once they appear, they are of very low amplitude. This suggests that the recombination rate is greater than the diffusion rate of the turbulent wake and that the electrons scattering from the small viscous core give all of the return. The return fluctuates since the free electrons causing the scattering are in groups within individual eddies of the viscous wake.

The effect of pressure and velocity is shown in Figure 6. Comparison of four 5-Gcs reflected returns can be made, and the difference in fluctuations between the two tests made at 1.0 mm Hg and the two at 10 mm Hg is easily seen. From luminosity measurements it has been determined that laminar-to-turbulent transitions occur well behind the body at 1.0 mm Hg, while at 10 mm Hg the transition occurs at the body. One explanation for the "roughness" of the return at 10 mm Hg is that the turbulent wake disturbs the ionized wake. The differences in amplitude of the tests at the same pressure can be attributed to the velocity difference (1100 ft/sec).

Decay half-lifes have been plotted[4] and transition possibility noted as a function of velocity. Radical change-of-decay time is observed at a particular velocity at a constant pressure of 1 mm Hg.

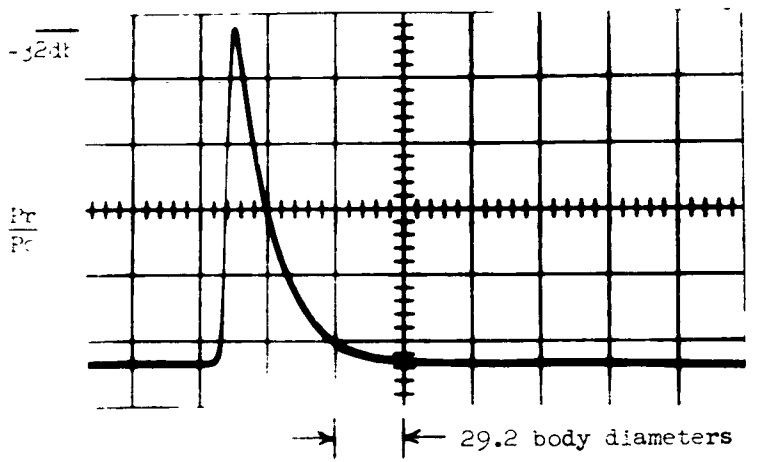

Laminar to turbulent transition well behind body.
1.0 mm Hg

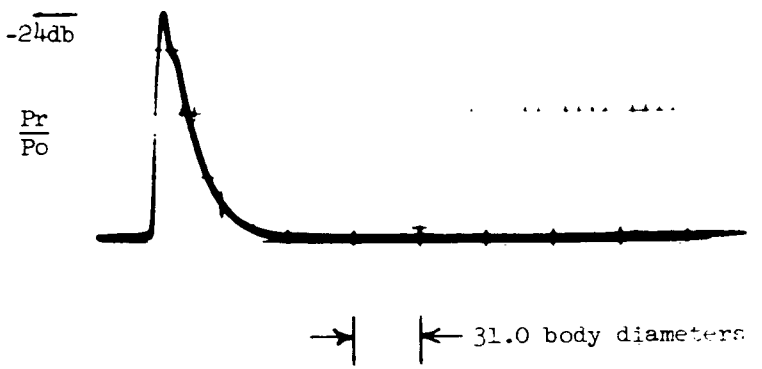

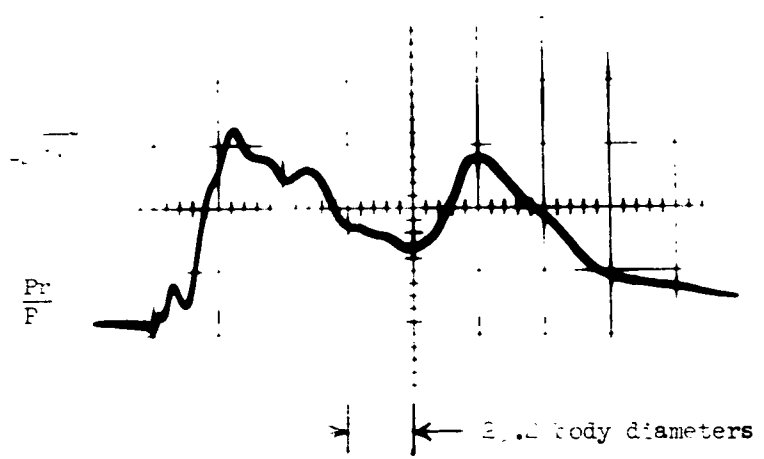

Initially Turbulent Wake

10.0 mm Hg

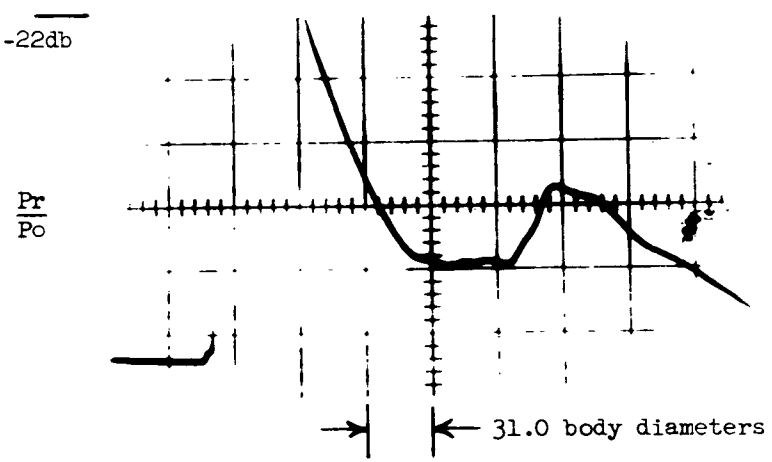

locity; 19,500 ft/sec

Velocity; 20,600 ft/sec

ure 6. Effect of Velocity and Pressure on Reflected Returns. Roughness is noted on initially turbulent trails.

IV. SUMMARY

Theoretical analysis of forward-scattered microwave signals from an ionized trail has led to an expression for charge (q) per unit length. The model derived appears to be valid for dilute plasma columns for many microwave frequencies. Analysis of forward-scattered returns is not dependent upon radial electron distributions. Estimates of ionized column diameters can be made from schlieren photographs, and comparison can be made of perfect scattering rod returns to trail returns in the overdense region. A region of uncertainty exists between the overdense and dilute columns that can be resolved by using multiple frequencies. Radial electron distribution determination may be possible by analysis of reflected signals at multiple frequencies. Theoretical work is directed to this solution.

Decay rate changes on microwave returns are observed on many tests and are similar to decay rate changes observed on radiation intensity measurements by Hidalgo. Direct correlation of RF decays to radiation intensity decays in the 3300-4000Å band has been made on several firings. Radar measurements to obtain the laminar-to-turbulent transition point or the altitude of transition appears quite possible.

Scattering from a turbulent wake has been observed to be quite different from scattering by a laminar wake. A smoothly varying return is seen from the laminar wake, while the turbulent wake appears to "roughen" the radar signal. If the scattering from a turbulent wake arises from individual eddies, a direct correlation may be possible by comparing RF returns to schlieren photos of the flow field.

A macroscopic model of an ionized wake may be valuable even though the interaction of a wake with RF energy is not completely understood. Features in the radar returns can be compared to the better understood radiation in the optical region to provide valuable information about laminar-to-turbulent transition, transition altitude, and scattering center separations. Insight may be derived from the macroscopic model to evolve a better theory for the phenomena associated with hypervelocity bodies.

V. FUTURE PROGRAM

A series of tests are planned to substantiate the conclusions presented in the previous section. The tests will follow the same lines as experiments already conducted but with an emphasis placed on particular areas. More details of the initial part of the wake are required to narrow down the transition point of laminar-to turbulent flow. Expanded time records of the measurements are expeditious to this detailed analysis. All parameters will be recorded on all firings so correlation may be made between optical and radar signatures. Measurements in the 2- to 7-micron band will be made by a recently installed IR detector.

Investigations will be made between non-ablative metal and ablative plastic projectiles to determine the effects of model ablation upon the various signals. An evaluation of range contamination will be made by analysis of samples of range atmosphere taken just prior to firing. If evaluation shows contamination evident, methods will be employed to reduce the contamination, such as condensation by cooling coils.

REFERENCES

1. V. R. Eshleman, "The Mechanism of Radio Reflections from Meteoric Ionization," Stanford Univ. Electronics Research Laboratory Technical Report No. 49, 15 July 1952.

2. J. Barthel, "The Microwave Diagnosis of a Column of Ionized Gas," ZPh-096, May, 1961, General Dynamics/Convair.

3. H. Hidalgo, R. L. Taylor and J. C. Keck, "Transition from Laminar to Turbulent Flow in Viscous Wake of Blunt Bodies Flying at Hypersonic Mach Numbers," AVCO R.M. 218, May, 1961.

4. M. Schoonover, B. Siperly, W. Short, "Microwave Studies of Flow Field Around Hypervelocity Projectiles," ZPh-094, 30 June 1961, General Dynamics/Astronautics.

5. R. F. Whitmer, "Principles of Microwave Interactions with Ionized Media, Part 1, Plasma Resonance," The Microwave Journal, Feb. 1959.

APPENDIX A

SCATTERING OF MICROWAVE POWER FROM A POINT SOURCE BY A DILUTE PLASMA COLUMN ELECTRON SCATTERING THEORY

The analysis presented here is a slight modification of a part of reference 2. Details are shown to facilitate data interpretation, as related to the assumptions used in the analysis. It is believed that the assumptions used here are the same as those employed in reference 2. Results show the linear charge density and reflection coefficient are each decreased by the factor $\sqrt{2}$ when we pass from the plane wave illumination (reference 2) to point source illumination (the present case).

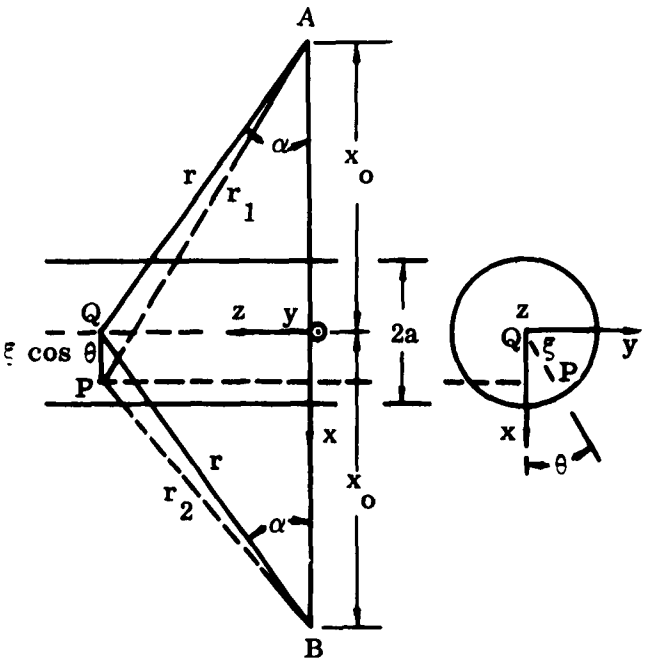

A unique feature of the present analysis is the demonstration that the results are insensitive to a reasonably slow axial dependence of radial charge distribution.

Assumptions to be Used

The figure above shows the geometry. A and B are phase centers of microwave horns polarized in the plane ABQ and pointed toward each other along the line AB. We suppose the horns are identical. Each has a principal E-plane (field) pattern $f(z) = f(-z)$ with $f(0) = 1$. The radiation field from A or

B is impressed on an electron at P. Radiation from the electron's harmonic motion is received at B. These fields are to be computed without regard to attenuation in the plasma. Hence we require that the skin depth, δ , of the plasma be related to its diameter, 2a, by the relation

$$\delta \gg 2a. \tag{A-1}$$

An order-of-magnitude estimate of the skin depth is obtained by inverting the attenuation constant for the uniform plasma as given, for example, by equation (27) of reference 5.

Geometric approximations to be employed are similar to those used in calculating patterns of linear antennas. For amplitude factors, the geometry becomes coplanar as point P is replaced by point Q. The assumption used is

$$2a \ll x_0 \tag{A-2}$$

A higher order approximation for r_1 and r_2 is required for phase applications. We shall be concerned with the phase angles $k(r_1 + r_2)$ and $2kr_2$. The same assumption, inequality (A-2), is applied to the exact relations,

$$r_1^2 = (\xi \sin\theta)^2 + z^2 + (x_0 + \xi\cos\theta)^2$$

and

$$r_2^2 = (\xi \sin\theta)^2 + z^2 + (x_0 - \xi\cos\theta)^2$$

to obtain

$$r_1 = r\left\{1 + \frac{x_0\xi}{r^2}\cos\theta + \frac{\xi^2}{r^2}\left(\frac{1 - \frac{x_0^2}{r^2}\cos\theta}{2}\right) + \cdots\right\}$$

and

$$r_2 = r\left\{1 - \frac{x_0\xi}{r^2}\cos\theta + \frac{\xi^2}{r^2}\left(\frac{1 - \frac{x_0^2}{r^2}\cos\theta}{2}\right) + \cdots\right\}$$

by the binomial expansion. Terms neglected above involve $(\xi/r)^n$ in which

$n \geq 3$. The error in the phase angles, $k(r_1+r_2)$ or $2kr_2$, introduced by dropping the third term in brackets, does not exceed $2k\xi^2/r \leq 2ka^2/x_0$. If we assert that this shall be very small compared to $\pi/2$, our third assumption becomes

$$(2a)^2 << \frac{\lambda x_0}{2} \qquad \text{(A-3)}$$

Assumptions (A-2) and (A-3) now permit us to write:

$$\left.\begin{aligned} r_1 &= r \\ r_2 &= r \end{aligned}\right\} \quad \text{(amplitude applications)}$$

$$\left.\begin{aligned} r_1 &= r + \frac{x_0 \xi}{r}\cos\theta \\ r_2 &= r - \frac{x_0 \xi}{r}\cos\theta \end{aligned}\right\} \quad \text{(phase applications)}$$

Forward-Scattered Analysis

On the basis of the remarks above the scalar magnitude of the radiation field at P, due to the source at A is

$$E_{1F}(\xi,\theta,z) = \frac{A f(z)}{r} e^{j(kr_1-\omega t)}$$

An electron at P, driven by this field, produces a scattered field of scalar magnitude

$$E_{2F}(\xi,\theta,z) = -\frac{\mu_0 e^2}{4\pi m}\cos(2\alpha)\frac{f(z)E_{1F}}{r} e^{jkr_2}$$

coupled into the antenna at point B. Let $N(\xi, z)$ be the electron density at P. The scalar magnitude of the scattered field at B, due to the entire

column of electrons, is

$$E_{SF} = \int_0^a \int_0^{2\pi} \int_{-\infty}^{\infty} E_{2F}(\xi,\theta,z) N(\xi,z)\, dz\, d\theta\, \xi\, d\xi \tag{A-4}$$

Now let

$$B \equiv -\frac{\mu_0 e^2}{4\pi m} A e^{-j\omega t} \tag{A-5}$$

$$F(\xi,z) \equiv N(\xi,z) f^2(z) \frac{\cos(2\alpha)}{r^2} \tag{A-6}$$

$$\Phi(z) \equiv k(r_1 + r_2) = 2kr \tag{A-7}$$

$$G_1(\xi,\theta) \equiv \int_{-\infty}^{\infty} F_1(\xi,z)\, e^{j\Phi(z)}\, dz \tag{A-8}$$

Equation (A-4) can now be written

$$E_{SF} = B \int_0^a \int_0^{2\pi} G_1(\xi,\theta)\, d\theta\, \xi\, d\xi. \tag{A-9}$$

The integration of equation (A-8) is performed by Kelvin's stationary phase method. We note that since $\cos 2\alpha = \cos^2\alpha - \sin^2\alpha$

$$F_1(\xi,z) = \frac{N(\xi,z)}{X_0^2} f^2(z) \frac{1 - \frac{z^2}{X_c^2}}{\left(1 + \frac{z^2}{X_0^2}\right)^2}$$

Also

$$\varphi(z) = 2k\left(x_o^2 + z^2\right)^{1/2}$$

$$\varphi'(z) = 2kz\left(x_o^2 + z^2\right)^{-1/2}$$

$$\varphi''(z) = 2kx_o^2\left(x_o^2 + z^2\right)^{-3/2}$$

The Taylor expansion of $\varphi(z)$ about its stationary point, $z = 0$, becomes

$$\varphi(z) = 2kx_o + 0 + \frac{kz^2}{x_o} + \cdots .$$

Equation (A-8) becomes

$$G_1(\xi,\theta) = \frac{N(\xi,0)}{x_o^2}\, e^{j2kx_o} \int_{-\infty}^{\infty} e^{jkz^2/x_o}\, dz .$$

The change of variable $z = (\sqrt{x_o\lambda}/2)u$ gives

$$\int_{-\infty}^{\infty} e^{jkz^2/x_o}\, dz = \sqrt{x_o\lambda} \int_{o}^{\infty} e^{j\frac{\pi}{2}u^2}\, du = \sqrt{\frac{x_o\lambda}{2}}\, e^{j\frac{\pi}{4}} .$$

Finally we have

$$G_1(\xi,\theta) = \frac{N(\xi,\theta)}{x_o}\sqrt{\frac{\lambda}{2x_o}}\, e^{j\left(2kx_o + \frac{\pi}{4}\right)} . \qquad \text{(A-10)}$$

Substitution of (A-5) and (A-10) in (A-9) gives

$$E_{SF} = -\frac{\mu_o e^2}{4m}\left(\frac{A}{2x_o}\right)\frac{2\theta}{\pi}\sqrt{\frac{\lambda}{2x_o}}\, e^{j\left(2kx_o + \frac{\pi}{4} - \omega t\right)} . \qquad \text{(A-11)}$$

where

$$q \equiv \int_0^a \int_0^{2\pi} N(\xi,0)\,\xi\,d\theta\,d\xi \qquad \text{(A-12)}$$

is the linear charge density in electrons/meter.

The direct radiation from the source at A is not balanced out in the plumbing associated with the receiving horn at B. The scalar magnitude of this radiation field is

$$E_{DF} = \frac{A}{2X_o}\, e^{j(2kX_o - \omega t)}$$

The sum of the direct and forward scattered fields at B is

$$E_F \equiv E_{DF} + E_{SF}$$

$$= E_{DF}\left\{1 - \frac{\mu_o e^2}{4m}\sqrt{\frac{\lambda}{2X_o}}\,\frac{2q}{\pi}\, e^{j\frac{\pi}{4}}\right\}.$$

The ratio of power received with the wake present to that without the wake is

$$\frac{P_f}{P_{f_c}} = \frac{|E_F|^2}{|E_{DF}|^2}$$

$$= 1 - \frac{q}{C} + \frac{1}{2}\left(\frac{q}{C}\right)^2,$$

where

$$C \equiv \frac{\pi}{2}\left(\frac{4m}{\mu_o e^2}\right)\sqrt{\frac{X_c}{\lambda}} = 1.8\sqrt{\frac{X_c}{\lambda}} \times 10^{12}\ \text{electrons/cm.} \qquad \text{(A-13)}$$

If we write

$$\left(\frac{q}{C}\right)^2 - 2\left(\frac{q}{C}\right) + 1 = 2\left(\frac{P_f}{P_{f_o}} - \frac{1}{2}\right)$$

it follows that

$$q_1 = C\left\{1 - \sqrt{2\left(\frac{P_f}{P_{f_o}} - \frac{1}{2}\right)}\right\} \qquad \text{(A-14)}$$

$$q_2 = C\left\{1 + \sqrt{2\left(\frac{P_f}{P_{f_o}} - \frac{1}{2}\right)}\right\}$$

Only the first of these two solutions is physically meaningful. This is because q_1 increases as the column dissipates and $P_f \rightarrow P_{fo}$ from below. Whenever $P_f < P_{fo}/2$ the remaining solution, q_1, becomes complex. It follows that the analysis is limited to charge densities which do not exceed

$C = 1.8\sqrt{x_o/\lambda} \times 10^{12}$ electrons/cm.

Back Scattered Analysis

In this case the antenna at B in the figure serves both as radiator and collector. By analogy with the previous section we have

$$E_{1B}(\xi, \theta, z) = \frac{A f(z)}{r} e^{j(kr_2 - \omega t)},$$

$$E_{2B}(\xi, \theta, z) = -\frac{\mu_o e^2}{4\pi m} \cdot \frac{f(z) E_{1B}}{r} e^{jkr_2}$$

and

$$E_{sB} = \int_0^a \int_0^{2\pi} \int_{-\infty}^{\infty} E_{2B}(\xi, \theta, z) N(\xi, z) \, dz \, d\theta \, \xi \, d\xi . \tag{A-15}$$

Let

$$B \equiv -\frac{\mu_c e^2}{4\pi m} A e^{-j\omega t}$$

$$F_2(\xi, z) \equiv \frac{N(\xi, z)}{r^2} f^2(z) \tag{A-16}$$

$$\psi(z) \equiv 2k r_2 = 2k\left(r - \frac{x_0 \xi}{r} \cos\theta\right) \tag{A-17}$$

$$G_2(\xi, \theta) \equiv \int_{-\infty}^{\infty} F_2(\xi, z) e^{j\psi(z)} dz . \tag{A-18}$$

Equation (A-15) can now be written

$$E_{sB} = B \int_0^a \int_0^{2\pi} G_2(\xi, \theta) \, d\theta \, \xi \, d\xi . \tag{A-19}$$

The stationary phase integration of equation (A-18) is similar in method to the integration of equation (A-8). Corresponding to equation (A-10) we have

$$G_2(\xi, \theta) = \frac{\frac{N(\xi, 0)}{x_0}\sqrt{\frac{\lambda}{2x_0}}}{\sqrt{1 - \frac{\xi}{x_0}\cos\theta}} e^{j\left[2k(x_c - \xi\cos\theta) + \frac{\pi}{4}\right]}$$

$$= \frac{N(\xi, 0)}{x_0}\sqrt{\frac{\lambda}{2x_0}}\left\{1 + \frac{\xi\cos\theta}{2x_0} + \cdots\right\} e^{j\left[2k(x_c - \xi\cos\theta) + \frac{\pi}{4}\right]} . \tag{A-20}$$

According to assumption (A-2), however,

$$\xi\,|\cos\theta|/(2x_c) \leq \frac{a}{2x_c} \ll \frac{1}{4}$$

It follows that equation (A-20) reduces to

$$G_2(\xi,\theta) = \frac{N(\xi,0)}{x_c}\sqrt{\frac{\lambda}{2x_c}}\; e^{j\left[2k(x_c-\xi\cos\theta)+\frac{\pi}{4}\right]}$$

When this is substituted in equation (A-19) we have

$$E_{sB} = -\frac{\mu_0 e^2}{4m}\sqrt{\frac{\lambda}{2x_c}}\;\frac{A}{\pi x_c}\; I\, e^{j\left(2kx_c+\frac{\pi}{4}-\omega t\right)} \qquad \text{(A-21)}$$

where

$$I \equiv \int_0^a\int_0^{2\pi} N(\xi,0)\, e^{-j2k\xi\cos\theta}\, d\theta\,\xi\, d\xi.$$

Since, however,

$$e^{-jz\cos\theta} = J_0(z) + 2\sum_{n=1}^{\infty}(-j)^n J_n(z)\cos(n\theta),$$

it follows that

$$I = 2\pi\int_0^a N(\xi,0)\, J_0(2k\xi)\,\xi\, d\xi. \qquad \text{(A-22)}$$

Esnleman's "reflection coefficient", defined in the text, can be written in our present terminology as

$$\rho_B \equiv \sqrt{\frac{\pi k x_c}{2}}\cdot\frac{|E_{sB}|}{|E_{iB}(0,\theta,0)|}. \qquad \text{(A-23)}$$

Substitution of equations (A-21) and (A-22), and

$$|E_{iB}(0,\theta,0)| = A/x_c$$

in equation (A-23) gives

$$\rho_B = \frac{1}{\sqrt{2}}\left(\frac{\mu_0 e^2\pi}{2m}\right)\int_0^a N(\xi,0)\, J_0(2k\xi)\,\xi\, d\xi. \qquad \text{(A-24)}$$

Equations (A-14) and (A-24) are identical to the corresponding results in reference 2, except that q and ρ_a have been reduced by the factor $\sqrt{2}$. This reduction factor is the one expected to accompany the change from plane wave to point source illumination.

APPENDIX P

PROPAGATION WITHIN THE PLASMA

The present discussion deals with the relations which must exist among the plasma parameters in order that free-space calculations can be used to describe electric fields which penetrate a plasma column to interact with individual electrons within the column. Thus, the procedure used in Appendix A assumes that the plasma's propagation constant, $\alpha + j\beta$, has attenuation constant with magnitude $-\alpha \ll \beta_c$ and phase shift constant, $\beta \rightarrow \beta_c$ Here $\beta_c \equiv \omega/c$. The plasma parameters to be limited in relation to the microwave frequency, $\omega/(2\pi)$, are the plasma frequency, $\omega_p/(2\pi)$, and the frequency, ν , with which the average electron collides with neutral particles.

For simplicity, consider the plasma as a uniform unbounded medium having relative dielectric constant,

$$K_1 + j K_2 = K e^{j\varphi} \tag{B-1}$$

in which K_1, K_2, K and φ are real. The propagation constant and relative dielectric constant are related by the equation

$$\alpha + j\beta = j\beta_c \sqrt{K_1 + jK_2} \tag{B-2}$$

from which

$$\frac{\beta}{\beta_c} = \sqrt{K} \cos\frac{\varphi}{2} = \sqrt{\frac{K + K_1}{2}} \tag{B-3}$$

and

$$-\frac{\alpha}{\beta_c} = \sqrt{K} \sin\frac{\varphi}{2} = \sqrt{\frac{K - K_1}{2}}$$

Notice $\beta/\beta_c > 0$ and $\alpha/\beta_c < 0$ to agree with the $e^{-j\omega t}$ time dependence of fields. Since we must have $\beta/\beta_c \to 1$ and $-\alpha/\beta_c \ll 1$, it follows that

$$0 \leq \tan\left(\frac{\varphi}{2}\right) \ll 1. \tag{B-4}$$

Equations B-7 will show K_1 can be, in general, either positive or negative while K_2 must always be positive. The left-hand inequality above shows the (overdense) case, when $K_1 < 0$, is not permitted in the present treatment.

It should not be supposed that propagation is impossible in the overdense case. In fact, when $K_1 < o$, equations (B-3) yield

$$\frac{\beta}{\beta_c} = \sqrt{\frac{-K_1}{2}\left(\sqrt{1+\left(\frac{K_2}{K_1}\right)^2} - 1\right)} \quad \text{and}$$

$$-\frac{\alpha}{\beta_c} = \sqrt{\frac{-K_1}{2}\left(\sqrt{1+\left(\frac{K_2}{K_1}\right)^2} + 1\right)}$$

These are both real. We exclude $K_1 < o$ because this was implicit in the treatment selected for Appendix A.

The right hand inequality, in inequalities (B-4), shows the need for a small loss tangent. This implies the only expansion for K, useful for our present problem, is

$$K = \sqrt{K_1^2 + K_2^2} = K_1\left\{1 + \frac{1}{2}\left(\frac{K_2}{K_1}\right)^2 - \frac{1}{8}\left(\frac{K_2}{K_1}\right)^4 + \cdots\right\}.$$

When this is substituted in equations (B-3), the latter reduce to

$$\frac{\beta}{\beta_c} = \sqrt{\frac{K+K_1}{2}} = \sqrt{K_1}\left\{1 + \frac{1}{2}\left(\frac{K_2}{2K_1}\right)^2 + \cdots\right\}$$

$$-\frac{\alpha}{\beta_0} = \sqrt{\frac{K-K_1}{2}} = \sqrt{K_1}\left(\frac{K_2}{2K_1}\right)\left\{1 - \frac{1}{2}\left(\frac{K_2}{2K_1}\right)^2 + \cdots\right\} \qquad \text{(B-5)}$$

with $K_1 > 0$.

The attenuation and phase-shift requirements stated in the first paragraph can now be restated in terms of parameters more directly comparable with the plasma parameters. We how have

$$\sqrt{K_1} \longrightarrow 1$$

and

$$\frac{K_2}{2K_1} \ll 1. \qquad \text{(B-6)}$$

The plasma parameters are related to the relative dielectric constant by equation (24) of reference (5).

Thus

$$K_1 = 1 - \frac{\omega_p^2}{\omega^2+\nu^2}$$

and

$$K_2 = \frac{\nu}{\omega} \cdot \frac{\omega_p^2}{\omega^2+\nu^2}. \qquad \text{(B-7)}$$

Now let

$$\frac{\omega_p^2}{\omega^2+\nu^2} \ll 1$$

and

$$\frac{\nu}{2\omega} \lesssim 1. \qquad \text{(B-8)}$$

It then follows that

$$\sqrt{K_1} = 1 - \frac{\omega_p^2/2}{\omega^2+\nu^2} + \cdots$$

and

$$\frac{K_2}{2K_1} = \frac{\nu}{2\omega}\frac{\omega_p^2}{\omega^2+\nu^2}\left\{1 + \frac{\omega_p^2}{\omega^2+\nu^2} + \cdots\right\}. \qquad \text{(B-9)}$$

We conclude that inequalities (B-6) are satisfied provided inequalities (B-8) are. Finally, we can substitute equations (B-9) in equations (B-5) and save only the terms which are significant when (B-8) are satisfied. We have

$$\frac{\beta}{\beta_0} = 1 - \frac{\omega_p^2/2}{\omega^2+\nu^2} \longrightarrow 1$$

and (B-10)

$$-\frac{\alpha}{\beta_0} = \frac{\nu}{2\omega}\,\frac{\omega_p^2}{\omega^2+\nu^2} \ll \frac{\nu}{2\omega} \leqslant 1$$

Expressions (B-10) establish that inequalities (B-8) are, in fact, the plasma limitations necessary so that the analysis of Appendix A applies without modification.

An empirical relation given by reference (5) enables us to go one step further. If p is the ambient pressure in mm Hg we have

$$\nu \approx 6\times10^{9}\,p \ \text{sec}^{-1}, \tag{B-11}$$

for hydrogen. Suppose the collision frequency depends only on the neutral particle density. Then, at low pressures, this is determined by the perfect gas law. On this basis equation (B-11) is applied to rarified air. Inequalities (B-8) can now be written

$$\frac{(f_p/f)^2}{1+0.91\left(\frac{p}{f\times10^{-9}}\right)^2} \ll 1 \tag{B-12}$$

and

$$p \leqslant 2.1\,(f\times10^{-9}).$$

Here $f_p \equiv \omega_p/(2\pi)$ and $f \equiv \omega/(2\pi)$ are plasma and microwave frequencies, respectively, and p is the ambient pressure in mm Hg.